Chapter

Flexible Porous Carbon Nanotube Films Intercalated with Active and Functional Materials for Lithium-Ion Batteries

Xiaogang Sun, Xu Li, Wei Chen, Jie Wang, Chengcheng Wei, Yapan Huang, Guodong Liang and Hao Hu

Abstract

Lithium-ion battery (LIB) has occupied the main position of portable electronic devices, and it is also playing an important role in energy storage and large energy storage. Thin film devices based on their diverse functions have great potential for wide application. Novel thin film devices need to be created for the improvement of electrochemical performance and safety of LIB. Our research focused on transparent conductive films and new flexible porous carbon nanotube films for improving and enhancing the energy/power density and cyclic performance of LIB. Meanwhile, different carbon nanotube films have their own additional advantages in strength and thermal conductivity to meet various functional requirements of LIBS.

Keywords: carbon nanotubes, lithium-ion battery, cellulose, film, collector

1. Introduction

At present, fossil energy has been overexploited and overutilized. Traditional fuels are not only facing depletion of reserves but also causing serious air pollution and endangering human health. Comfortable, fresh, green, and pollution-free living environment has become the urgent need of humans [1–5]. Now energy problem and environmental protection have become two important issues in the world. With the rapid development of portable electronic equipment and transportation tools, many countries have devoted a lot of human and material resources to the development of high-performance energy storage devices [6–12] with low consumption and that are pollution-free.

Thin film devices have so many functions which can be conductive, magnetic, luminous, catalytic, antibacterial, sound insulated, and flame retardant and other characteristics after compounding with different functional materials that are widely used in antistatic packaging materials, electromagnetic shielding materials, new energy and electrochemical materials, heating materials, and sensing and braking materials [13–28] and other fields. For example, transparent conductive film has been extensively used in flat panel displays, solar cells, and touch panels and other fields because of its conductive and light transmission characteristics

[29–31]. However, commercial thin film devices which are widely used nowadays have high cost and poor bending resistance, so it is necessary to create new thin film devices.

It has been 20 years after the discovery of carbon nanotubes (CNTs) by Japanese scientist Iijima in 1991 [32]. CNTs have become a hot carbon material for researchers to explore and develop its wider range of properties and applications actively. It is found that CNTs are one-dimensional materials with seamless, hollow, and single-walled or multi-walled tubular structures and curled by graphite [33–40]. CNTs have excellent electrical and mechanical properties, high aspect ratio, and good lithium insertion performance. Carbon nanomaterial-based transparent conductive films have good electrical conductivity, outstanding chemical stability [27, 29, 41–44], good substrate adhesion, and excellent mechanical flexibility and can be produced in large quantities and suitable for continuous filmmaking, which make CNTs occupy an important position in the field of new thin film devices, especially in the field of flexible transparent conductive films. And CNTs were also the earliest carbon nanomaterials [30, 37, 45–48] used to study transparent conductive films. Nowadays, the commercial production of CNTs has been very perfect. But CNTs are nanoscale materials, with large specific surface area and high surface energy, so CNTs show significant agglomeration effect. In addition, CNTs are one-dimensional fibrous nanomaterials with large length/diameter ratio, which makes CNTs have intertwined and binding properties similar to that of fibers. The interaction of the two properties makes CNTs form stable aggregates, affecting their further commercialized application [47, 49]. In order to solve this problem, researchers have searched for many methods of decentralization. Physical dispersion methods include grinding, ball milling, ultrasonic oscillation, high-speed shearing, and so on [37, 38, 48–50]. Chemical dispersion methods include washing with strong acid and strong base and adding surfactant dispersant [51–54]. However, all the dispersion methods have their limitations, so it is difficult to obtain a stable carbon nanotube dispersion solution. Therefore, it is necessary to develop better dispersion methods or to make a kind of easily dispersed carbon nanotubes for better application in the development of thin film devices.

In this work, we have created a method for manufacturing carbon nanotubes which can be dispersed easily (WhiskerCNT). Carbon nanotube transparent conductive film (WTF), flexible porous carbon nanotubes films (FWFs), and active conductive film fabricated by WhiskerCNT have good physical and chemical properties.

2. Preparation and characterization of WhiskerCNT

2.1 Fabrication of WhiskerCNT

Benzene was used as carbon source. Ferrocene was used as catalyst, and thiophene was added into benzene to stir evenly. The input rate of raw materials is controlled by a micro pump. The carrier gas was composed of hydrogen and argon, and the gas flow velocity was controlled by a mass flowmeter. The reaction was carried out in a vertical furnace, and the preparation was carried out at a certain temperature gradient (the detailed production process is described in the corresponding patent of our research group). The purity of WhiskerCNT obtained by preliminary production is 95–97%, and further graphitization is needed to improve the purity.

WhiskerCNT was placed in a graphitizing furnace, and high purity argon was introduced as a protective gas after vacuum extraction. When the furnace is cooled, WhiskerCNT can be removed. Then the purity can be over 99.6%.

2.2 Characterization of WhiskerCNT

Figure 1 is the morphological characterization of graphitized WhiskerCNT. WhiskerCNT is linear tubular structures with relatively small transverse lengths and large aspect ratios, and it is mainly distributed in a straight line, which makes the chances of bending and winding between WhiskerCNT and pipes small and easy to disperse (**Figure 1a**). WhiskerCNT diameter is about 50 nm. The nanotubes have a thin cavity in the middle. The layered structure of the tube wall is clear and orderly (**Figure 1b**), and the interval is 0.338 nm by calculating wall thickness and stories.

Figure 2 is the characterization of graphitized WhiskerCNT. The sharp diffraction peaks of graphitized WhiskerCNT show that WhiskerCNTs have high crystallinity (**Figure 2a**). The D peak of Raman pattern is very low, indicating that WhiskerCNTs have a complete structure and an orderly arrangement (**Figure 2b**). The G peak is sharp, and the I_G/I_D is up to 16.95, which proves that WhiskerCNT has high graphitization degree and high purity.

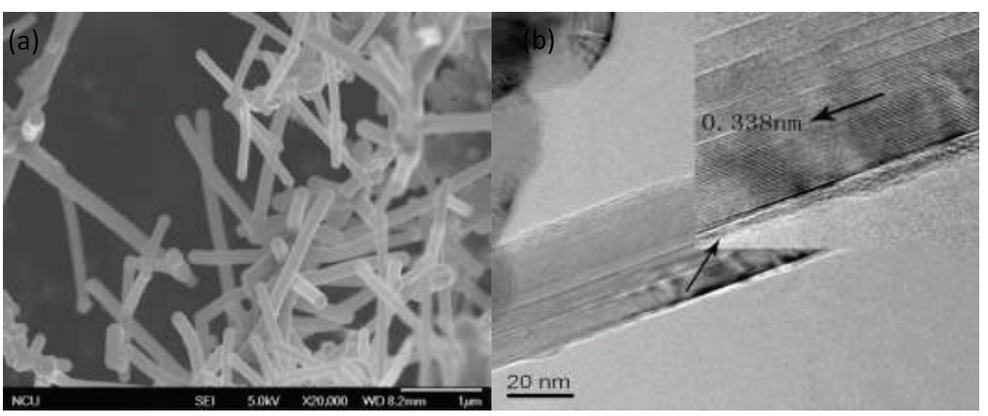

Figure 1.
Morphological characterization of graphitized WhiskerCNT: (a) SEM and (b) TEM.

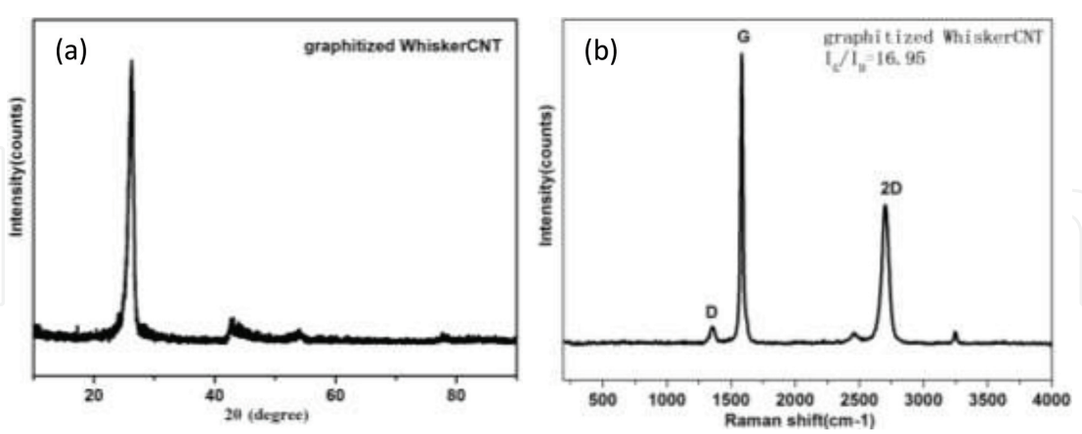

Figure 2.
XRD pattern (a) and Raman pattern (b) of graphitized WhiskerCNT.

3. WhiskerCNT transparent conductive films (WTF)

3.1 Preparation of WTF

The WhiskerCNT and graphitized WhiskerCNT were milled 2 h in a ball mill (200 r/min) to obtain fine powders. Two kinds of conductive fluids were prepared by adding the ball-milled WhiskerCNT (1 wt%) to ethanol with TNADIS (0.05 wt%)

and ultrasonic treating for 30 min and high-speed shearing for 1 h. The two conductive fluids were coated on the transparent PET film by spin coating. After spin coating for 1, 2, and 3 min separately, they were put into a vacuum drying box to dry.

	Item	1 min	2 min	3 min
WhiskerCNT	Square resistance (kΩ/sq)	103.3	10.6	3.7
	Transmittance (%)	68.30	57.90	52.80
G-WhiskerCNT	Square resistance (kΩ/sq)	53.6	2.8	0.34
	Transmittance (%)	68.90	58.10	53.30

Table 1.
Square resistance and transmittance of WTF.

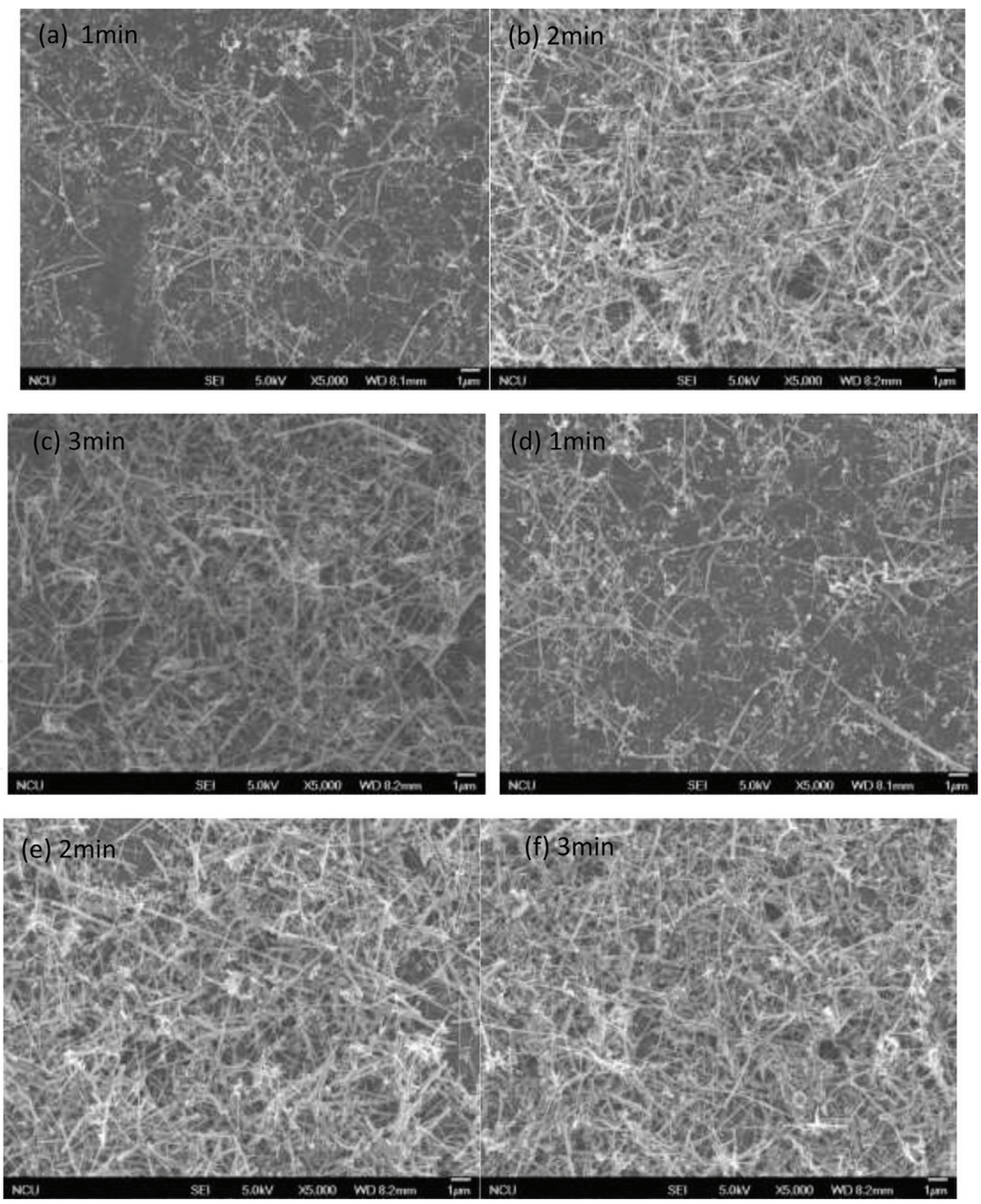

Figure 3.
SEM pattern of WTF. WhiskerCNT (a)–(c), graphitization WhiskerCNT (d)–(f).

3.2 Results and discussion

It is found from **Table 1** that the transmittance of the two films is similar, while the conductivity of G-WhiskerCNT WTF is stronger under the same spin coating time. With the increase of spin coating time, the transmittance of both films decreased, because WhiskerCNT gradually formed a continuous and dense network of electronic transmission paths from discontinuous interconnection (**Figure 3**).

4. Flexible porous WhiskerCNT films

In order to improve the electrochemical performance of lithium-ion batteries, a kind of flexible porous carbon nanotube films (FWFs) compounded of WhiskerCNT and cellulose fiber was prepared by process similar to papermaking method.

4.1 Preparation of FWF

Graphitized MWCNT powder was dispersed in deionized water by sonication for 2 h and followed by high-speed shearing for 2 h with an addition of sodium dodecylsulfate (SDS) as a surfactant. Cellulose pulp was prepared by immersing softwood pulp into deionized water and followed by high-speed shearing for 3 h. The MWCNT dispersion liquid and the cellulose pulp were mixed by high-shear emulsifier to form suspension for 3 h. The suspension liquid of cellulose and MWCNT pulp was infiltrated by vacuum filtration. A randomly interwoven fiber mat was obtained. The host was rolled and tailored for the activated materials.

4.2 Characterization of FWF

Figure 4(a) showed the SEM image of top surface of FWF with a random-in-plane weblike network structure. FWF host demonstrated homogenous incorporation of WhiskerCNT in the cellulose fiber network. **Figure 4(c)** showed the cross-sectional image of FWF. The figures clearly displayed porous network structure which provided sufficient void space for loading a large amount of active substance and accommodating the volume expansion of active substance during cycles. The coarse surface and interconnected channel permit good penetration of the electrolyte and active substance. WhiskerCNT is uniformly dispersed and attached on paper fiber (**Figure 4b**). A good three-dimensional conductive network was constructed with cellulose fiber as the framework and MWCNT as conductors. WhiskerCNTs have smaller nanostructures, so they fill, adsorb, and agglomerate on the surface of paper fibers and in the gap between paper fibers, acting as the carrier of paper fiber connection. FWF exhibited porous, flexible, and high specific surface area. Pore size distribution of FWF is shown in **Figure 4(d)**. From the picture, we can see the host has big porosity. The special surface area of FWF reached 25.6 m^2/g.

4.3 FWF as collector in ternary materials of lithium-ion battery

4.3.1 Preparation of positive electrode and half-cells

After milling WhiskerCNT, SDS (CNTs:SDS = 90 wt%:10 wt%) and NMP solvents were added and followed by high-speed shearing for 4 hours. The WhiskerCNTs were dispersed fully and prepared into 5% solid content WhiskerCNT

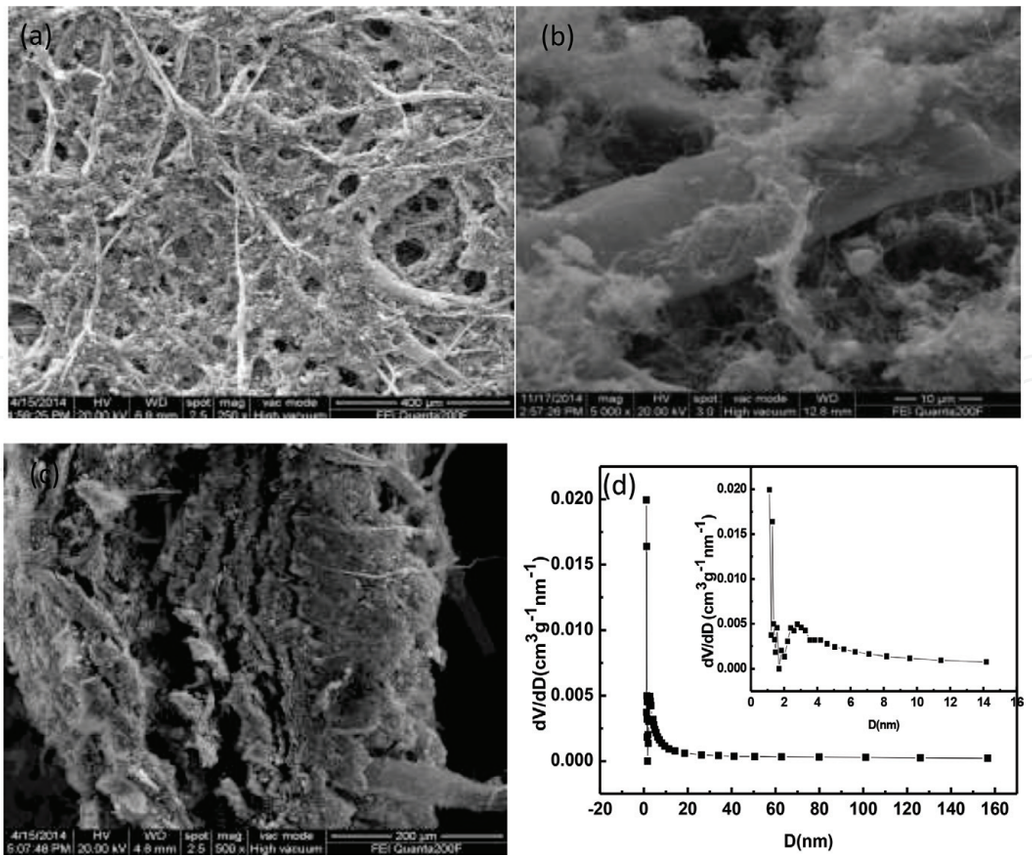

Figure 4.
SEM of FWF (a), (b). TEM of FWF (c). BET of FWF (d).

dispersion solution. In the proportion of LNCM:WhiskerCNT:PVDF = 90 wt%:5 wt %:5 wt%:5 wt%, ternary cathode active materials were prepared, in which WhiskerCNT came from the preceding configuration of carbon nanotube dispersion. The cathode slurry was prepared by placing the prepared material in a sealed test tube, adding an appropriate amount of NMP, ultrasonic treating for 0.5 h, and shearing for 0.5 h at a high speed of 10,000 r/min. The cathode paste was divided into two equal parts, coated on aluminum foil and FWF, and dried at 60C. In the vacuum glove box, two kinds of electrode plates were assembled into a button cell, and the electrochemical performance of the cell was tested.

4.3.2 Results and discussion

Aluminum foil and FWF were coated with LNCM paste to assemble the battery and test the electrochemical performance of the battery. **Figure 5** is a comparison of the first charge of lithium-ion batteries with two different collectors at a discharge voltage of 2.0–4.5 V at 0.1C. Among them, the first discharge-specific capacity of ternary/FWF electrode (a) is 184 mAh/g, and the first discharge-specific capacity of ternary/aluminum foil electrode (b) is 178 mAh/g. (a) relative to (b) the specific capacity increased by 3.3%. It shows that FWF instead of aluminum foil is the collector and has a certain specific capacity improvement effect at low magnification.

The SEM of **Figure 6** shows the microcosmic situation of three yuan doped with 5% CNTs. It is observed that the ternary spherical particles are completely coated by Whisker CNT and even stacked in some places. WhiskerCNTs are one-dimensional carbon nanomaterials with large aspect ratio, as shown in **Figure 6**. As a conductive agent, a three-dimensional space conductive network system is formed by interpolating and overlapping the carbon tube with the carbon tube.

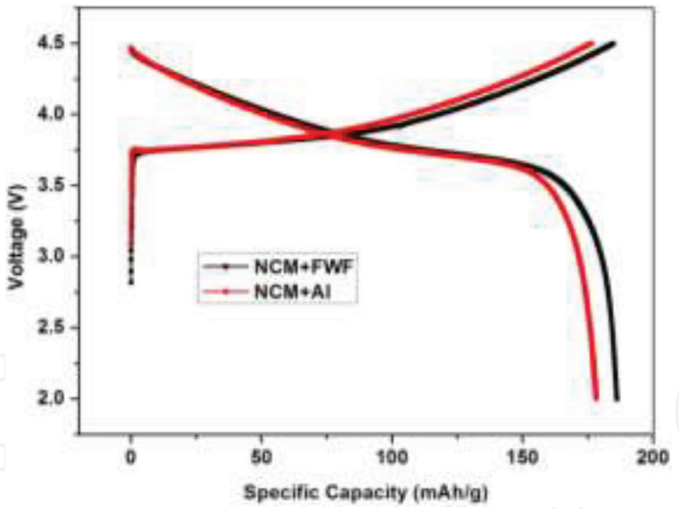

Figure 5.
First charge/discharge curves of two kinds of different collector electrodes.

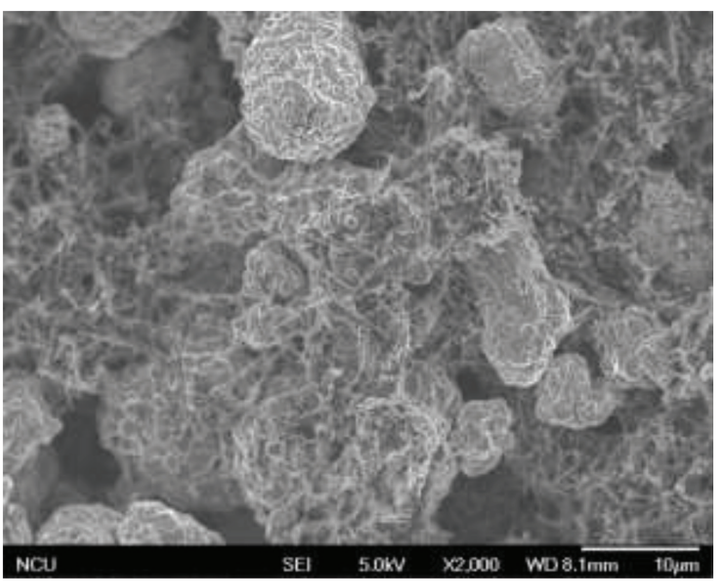

Figure 6.
SEM images of ternary cathode material doped with 5 wt% CNTs.

At the same time, the three-dimensional network is distributed among the ternary particles, conducting the electronic transmission between the ternary particles and the particles. Compared with the traditional super carbon black (SP), the way of conducting carbon nanotubes is extremely efficient. At the same time, the carbon nanotubes were duplicated in the experiment, the utilization rate was not maximized, and the content of carbon nanotubes could be reduced to reduce the cost. At the same time, it was found that the ternary cathode material on the ternary/aluminum foil electrode was easy to detach, while the ternary/FWF electrode was tightly bonded and difficult to separate. It shows that three yuan/FWF is more solid than three yuan/aluminum foils and the two composite effects are better. The reason is that the surface of aluminum foil is smooth, and the internal pores of conductive paper are abundant, and the adsorption is strong, so the ternary material after coating penetrates into the interior of conductive paper and bonds closely with conductive paper, while the aluminum foil can only be attached to the surface.

Figure 7 is the micrograph of ternary/aluminum foil electrode and ternary/FWF electrode. The reason why FWF is better than aluminum foil is analyzed. It can be seen from the observation (a) that, because the aluminum foil is smooth and flat,

the ternary coating on the aluminum foil contacts in the form of point to face, (a) fully showing that there is a large gap between the two interfaces due to this factor. In **Figure 7(b)** FWF, because of its uneven internal structure and rich pores, ternary materials penetrate into the interior of conductive paper, and ternary materials and conductive paper are closely combined. Therefore, the interfacial gap between ternary and FWF is basically absent in **Figure 7(b)**, showing a good interfacial bonding effect. Because of the advantages of interface performance, the three-element/FWF electrode has better electrochemical performance at low magnification.

The first 28 cycles of the 2 electrodes showed that the capacity retention rate of ternary/FWF electrode was 94% and that of ternary/aluminum foil electrode was 94% at 0.1C. But the curve in **Figure 8** shows that the specific capacity of the ternary/conductive paper electrode is higher than that of the ternary/aluminum foil electrode at a small rate, indicating that the specific capacity of the battery has been improved when FWF is used as a collector (the same information is shown in **Figure 5**).

The ratio performance diagram of ternary/FWF electrode is shown on the left and the ratio performance diagram of ternary/aluminum foil electrode on the right. At 0.1, 0.5, 1, 2, and 0.1C discharge, the specific capacities of ternary/FWF electrodes are 184, 155, 120, 120, and 160 mAh/g, and the specific capacities of ternary/aluminum foil electrodes are 178, 154, 138, 121, and 165 mAh/g. The specific capacity of ternary/FWF electrode was 184 mAh/g at 0.1C low rate, while that of

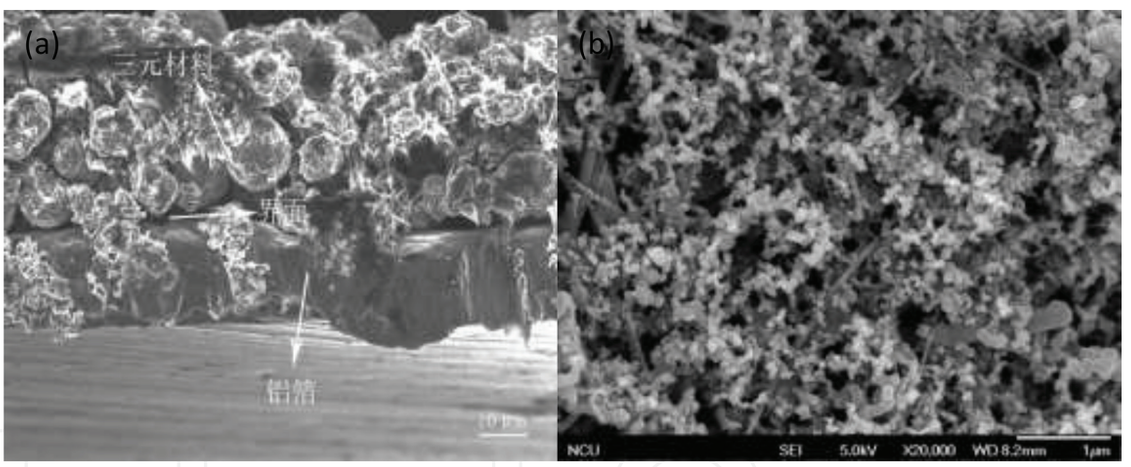

Figure 7.
(a) SEM image of NCM/aluminum foil electrode and (b) SEM image of NCM/FWF.

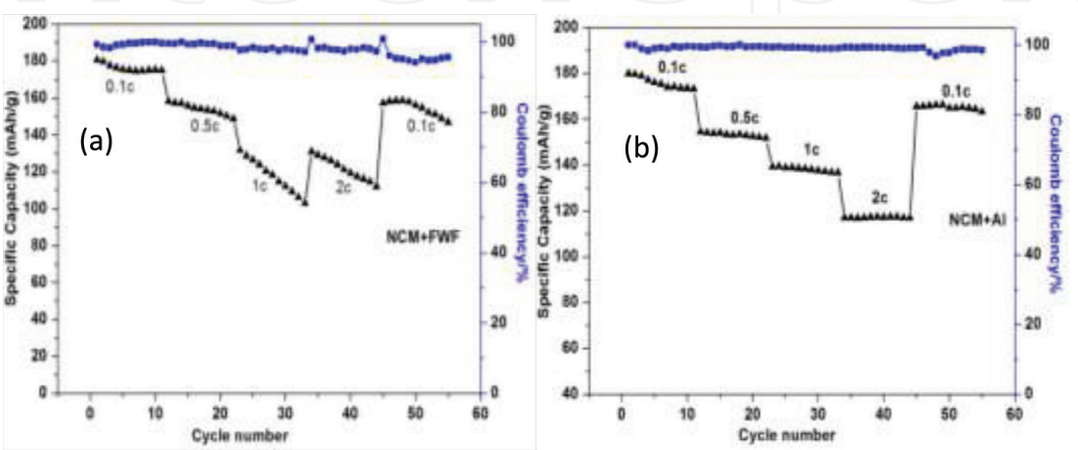

Figure 8.
Comparison of the two kinds of electrode's rate performance. NCM + FWF (a) and NCM + Al (b).

ternary/aluminum foil electrode was 178 mAh/g. However, at 1C and 2C high rate, the specific capacities of the ternary/conductive paper electrodes decreased to about 120 and 120 mAh/g, and the specific capacities of the ternary/aluminum foil electrodes remained good and tended to be stable at about 138 and 121 mAh/g. It shows that ternary/FWF is better than ternary/aluminum foil electrode at low magnification, but there are some shortcomings at high magnification. The reason is that FWF becomes looser and decomposed after a long time of electrolyte infiltration in the late period of each rate discharge, resulting in the increase of resistance of electronic transmission channel and the decrease of capacity. During the discharge of 1C and 2C, it was suspended for 1 minute. Because of the looseness and microelasticity of the FWF, the specific capacity of the battery was temporarily increased and then began to decay after a short recovery period of 1 minute, so the discharge of 2C reached 1C mode again, showing the phenomenon that the specific capacity of 2C was higher than that of 1C in the later period.

Figure 9 shows the impedance spectrum comparison of the two electrodes. The starting point of high-frequency region and the intersection point of real axis are the resistance in solution (Rs), the semicircle in intermediate frequency region is the charge transfer resistance (Rct) between SEI film and solid electrode, and the line in low frequency region is the diffusion resistance Zw of lithium ion in solid electrode material. It can be seen from observation that the Rs of the two batteries is basically the same. The Rct of ternary/FWF electrode is 175 and that of ternary/aluminum foil electrode is 275, indicating that FWF instead of aluminum foil as collector has a smaller charge transfer resistance, which is conducive to improving the electron migration rate and reaction depth during charging and discharging.

4.3.3 Conclusions

Graphitization treatment can improve the defects of carbon nanotubes, increase the degree of graphitization of carbon nanotubes, and make the arrangement of carbon atoms more orderly, which are conducive to the follow-up application. The initial specific capacity of ternary/FWF electrode is 184 mAh/g and that of ternary/aluminum foil electrode is 178 mAh/g at 0.1C, which is 3% higher than that of aluminum foil electrode. After 28 cycles, the capacity retention rate is above 94%.

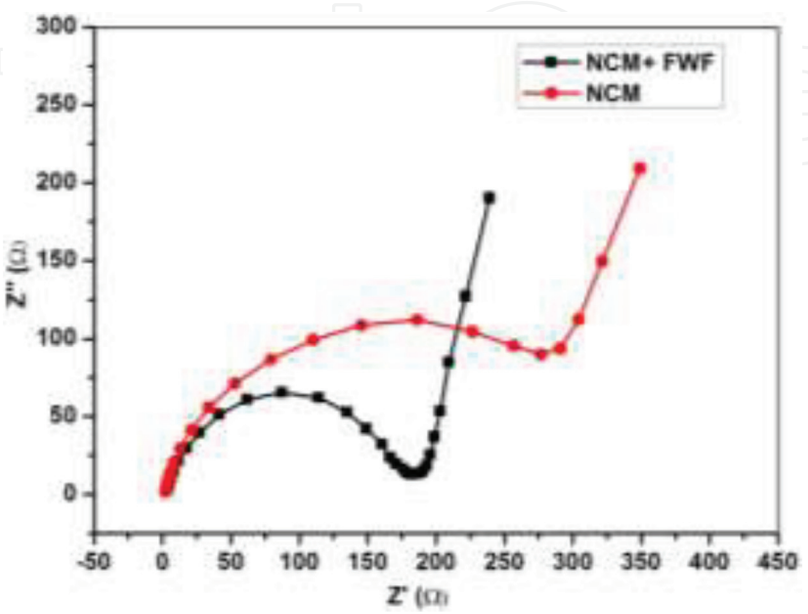

Figure 9.
Impedance spectra of NCM/conductive paper electrode and NCM/aluminum foil electrode.

At 1C and 2C high rate discharge, the specific capacities of ternary/FWF electrodes are 120 and 120 mAh/g and that of ternary/aluminum foil electrodes are 138 and 121 mAh/g. In contrast, the ternary/FWF electrodes have a greater attenuation because of the decomposition and shedding of FWF at the later stage, which needs to be solved. When FWF replaces aluminum foil as collector, the ternary/aluminum foil electrode Rct is 275, and the ternary/FWF electrode Rct is 175, which decreases by 36%, indicating that the impedance of the battery has been significantly improved. FWF instead of aluminum foil as collector has better interfacial performance; it makes ternary materials and collector substrate bond more closely, reduces the internal impedance of the battery, increases the specific capacity of ternary materials, and maintains better cycle performance, but the high rate performance needs to be improved.

4.4 FWF as collector in Li-Si battery

4.4.1 Preparation of electrode and half-cells

WhiskerCNT powders and hollow silicon were mixed and then were dispersed by sonication and high-speed cutting in distilled water for 2 h, respectively. The dispersant of polyvinylpyrrolidone (PVP) was added to improve the dispersion performance. The slurry of hollow silicon and WhiskerCNT was coated on the FWF.

CR2025 coin-type cells were assembled in an Ar-filled glove box with a metallic lithium foil as the counter electrode. The electrochemical performance was tested by a cell tester with 1 M $LiPF_6$ in a mixture of ethylene carbonate (EC) and diethyl carbonate (DEC) as electrolyte.

4.4.2 Results and discussions

In **Figure 10a**, it can be observed that the distribution of hollow silicon is chaotic and disordered, and get agglomeration phenomenon. While there is a different situation in **Figure 10b**, hollow Si can embed into micropores of FWF evenly. Micron-sized hollow silicon is evenly dispersed in the high-porosity grid consisted by WhiskerCNT and fiber, forming a similar coating effect (**Figure 10c**), which solves the problem of nonconductivity of Si and increases the storage channel of Li+. The active material can be well penetrated into the layered porous structure of FWF. At the same time, the WhiskerCNTs in active materials and in FWF are well connected, which makes the interface resistance to decrease, the electron transfer channel to increase, and the cell polarization effect to decrease, thus increasing the utilization rate of active materials. Si hollow microspheres are wrapped in layers by WhiskerCNT (**Figure 10d**), which can accommodate and buffer the volume expansion of Si. Moreover, FWF adsorbs the active material well so that active material is hard to crack or be separated from the current collector.

As shown in **Figure 11**, the first battery constant current discharge of 0.01 V, observed in the first discharge process to the long platform that disappeared in the subsequent cycle, corresponding to the SEI film, is achieved by irreversible reaction, which leads to the low efficiency of Coulomb in the loss rate and charging capacity. The copper collector silicon lithium-ion battery (CLIB) at a current density of 0.02C, has an initial discharge capacity of 869 mAh/g, and Kulun for the first time efficiency is 38%. The second discharge reduced to 364 mAh/g, from the beginning of the battery capacity little attenuation, Kulun time efficiency was between 86 and 89%. The more stable cycle performance is attributed to the large volume change of the hollow silicon, which does not break, and the rapid diffusion of lithium ion in the hollow structure silicon. Even so, the volume change of silicon

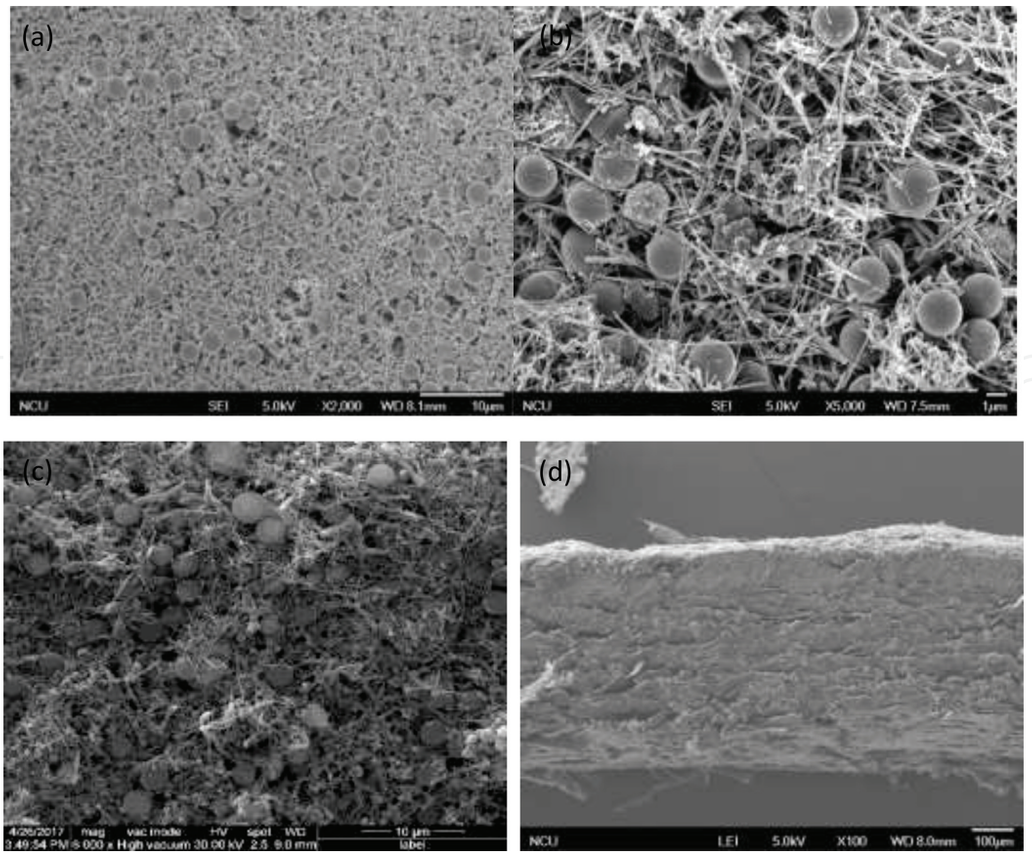

Figure 10.
SEM image of hollow Si-doped MWCNT compound material coated on copper foil (a), conductive paper (b, c), and its sectional drawing (d).

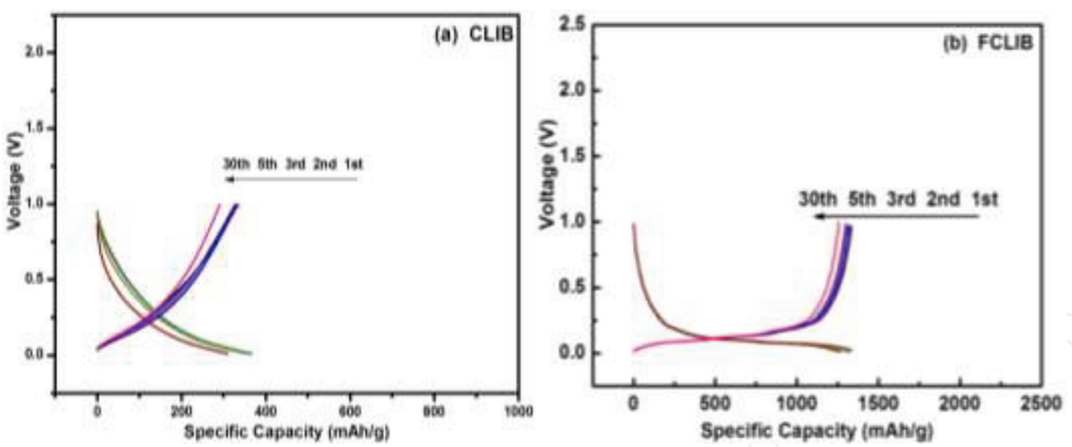

Figure 11.
Charging-discharging curve of CLIB (a) and FCLIB (b).

in the process of intercalation and debinding will lead to mutual extrusion and detachment between silicon particles. After repeated expansion and contraction, some silicon will even fall off from the copper foil collector. FWF collector for silicon-based lithium-ion battery (FCLIB) has an initial discharge capacity of 2168 mAh/g, and Kulun for the first time efficiency is 61.5%. The second discharge capacity is 1335 mAh/g, also from the second charge discharge start battery rapidly stable than capacity little attenuation, Kulun time efficiency are close to 100%, and cycle the 30 time was 1300 mAh/g, showed excellent discharge performance (**Figure 12**).

Under the current of 0.25C, PCLIB decreased continuously in the first eight times and then slowly reached 1150 mAh/g. When the small current density cycle is

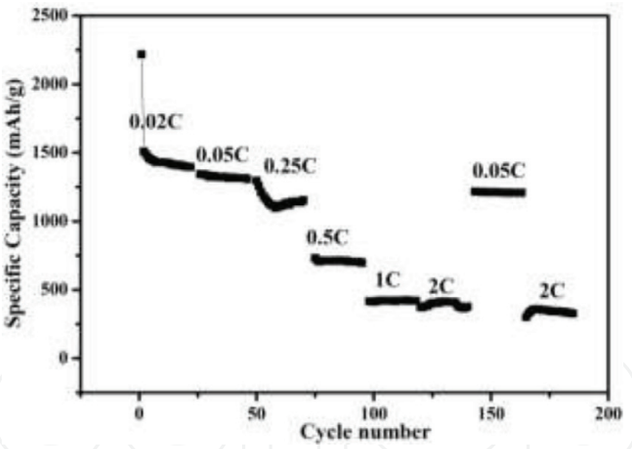

Figure 12.
Cyclic performance diagram of conductive paper battery under different current densities.

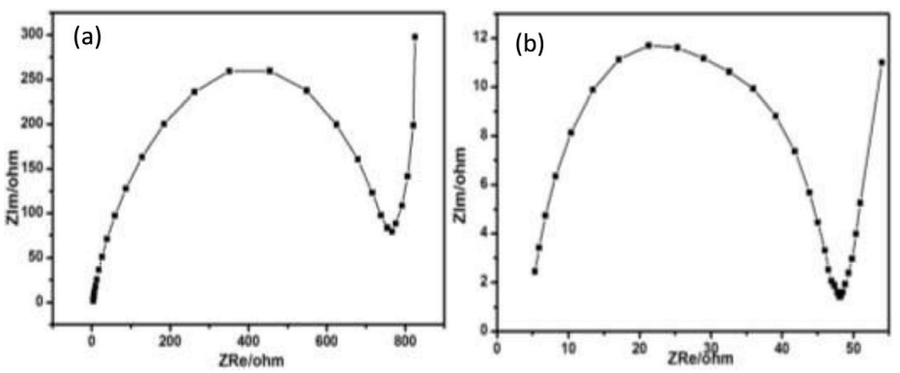

Figure 13.
EIS test diagram of conductive paper battery: predischarge (a) and after 30 cycles (b).

recovered, the specific capacity of CPLIB can be recovered to the original level. As figure PCLIB first circulated at the 2C current density for 30 times, it recovered to the 0.25C current, and the specific capacity recovered. This data shows the ability of PCLIB to maintain good specific capacity after repeated high current impact, long service life, and excellent cycling performance (**Figure 13**).

To better understand the volume change and the stability of SEI layer, the impedance analysis was performed. As shown in the picture, the contact resistance of the PSiLIB interface decreases significantly after the cycle. This is because the contact interface between active material and the collector will form a contact interface, which will cause greater resistance. As the reaction proceeds, the material will penetrate or compound to each other, and the contact surface will decrease or form the transition layer. The interaction of FWF with the WhiskerCNT in the active material enhances the conductivity of the active material and makes the resistance of the electrode smaller. In addition, the layered porous structure of CNT has the ability to adsorb and store the electrolyte stronger than the copper foil, which can make the reaction more complete and thorough.

4.4.3 Conclusions

In the summary, FWF was used as host of hollow Si for high-performance Li-ion battery. FWF has a porous structure and interconnected channel and exhibited high conduction and high absorption of electrolyte. Hollow Si

penetrated into the network of FWF and achieved a low interface resistance which contributed to the high rate performance of the battery. FWF with interconnected channel can absorb an amount of electrolyte and accommodate the volume expansion of hollow silicon to prevent the cracking and pulverization of hollow silicon in cycles. All those help to enhance electrochemical performance of FWF electrode. The good cycle performance was ascribed to the accommodation and buffering effect of FWF to huge volume expansion of silicon during cycles. Therefore, it was believed that FWF has a useful application prospect as current collector for high-performance silicon-based lithium-ion batteries.

4.5 Outlook for further improvement of FWF

In order to further improve the functionality and practicability of FWF, we used aramid fibers instead of paper fibers to make flexible porous WhiskerCNT films with ultrahigh strength and toughness (SFWF), polyimide fiber to make flexible porous WhiskerCNT films with high thermal conductivity (TFWF), and hydroxyapatite nanowires to make environmentally friendly multifunctional flexible porous WhiskerCNT films (EFWF).

Aramid fiber has excellent properties such as ultrahigh strength, high modulus, and high temperature resistance, acid and alkali resistance, and aging resistance, and insulation and has lightweight property, long life cycle, and so on. Its strength is 5–6 times that of steel wires, its toughness is 2 times that of steel wire, and its weight is only about 1/5 of that of steel wire. So it has been applied to many fields such as bulletproof products, special protective clothing, and so on. While SFWF produced by aramid fiber also has high strength, high toughness, and other properties by different kinds of performance testing. TFWF has higher thermal conductivity than FWF. Similarly, EFWF hydroxyapatite nanowires have high temperature resistance, corrosion resistance, and fire resistance and are an environmentally friendly and biocompatible material, because hydroxyapatite is the main inorganic component of vertebrate bones and teeth. Therefore, EFWF has wider application fields. The above three thin film devices have completed the preliminary performance testing, and further electrochemical performance testing needs to be carried out.

5. Conclusion and outlook

In summary, we reported our study of transparent conductive thin films and FWF for lithium-ion battery applications. It has great potential application value for lithium-ion battery, energy storage equipment, and other fields. Meanwhile, TFWF and EFWF have better physical and chemical properties than FWF. And we believe they have better application prospects.

Author details

Xiaogang Sun*, Xu Li, Wei Chen, Jie Wang, Chengcheng Wei, Yapan Huang, Guodong Liang and Hao Hu
School of Mechatronics Engineering, Nanchang University, Nanchang, China

*Address all correspondence to: xiaogangsun@163.com

IntechOpen

References

[1] Park S, Vosguerichian M, Bao Z. A review of fabrication and applications of carbon nanotube film-based flexible electronics. Nanoscale. 2013;**5**(5):1727

[2] Smith K, Wang CY. Power and thermal characterization of a lithium-ion battery pack for hybrid-electric vehicles. Journal of Power Sources. 2006;**160**(1):662-673

[3] Kennedy B, Patterson D, Camilleri S. Use of lithium-ion batteries in electric vehicles. Journal of Power Sources. 2000;**90**(2):156-162

[4] Zhong S, Hu J, Wu Z, et al. Performance of lithium ion batteries using a carbon nanotube film as a cathode current collector. Carbon. 2015; **81**:852

[5] Tang Z, He Y, Liu Y, et al. Effects of copper foil as cathode current collector on performance of Li-ion batteries. Corrosion Science and Protection Technology. 2007;**19**(4):265

[6] Jinjin Z, Shuxia R, Yan-liang D, et al. Study on the influence of carbon nanotubes on the mechanical properties of Portland cement. Bulletin of the Chinese Ceramic Society. 2013;**32**(7): 1361-1370

[7] Terrones M. Science and technology of the twenty-first century: Synthesis, properties, and applications of carbon nanotubes. Annual Review of Materials Research. 2003;**33**(1):419-501

[8] Yakobson BI, Avouris P. Mechanical properties of carbon nanotubes. Topics in Applied Physics. 2001:287-327

[9] Anderson RE, Guan J, Ricard M, et al. Multifunctional single-walled carbon nanotube-cellulose composite paper. Journal of Materials Chemistry. 2010; **20**(12):2400-2407

[10] Hu L, Choi JW, Yang Y, et al. Highly conductive paper for energy-storage devices. Proceedings of the National Academy of Sciences. 2009;**106**(51): 21490-21494

[11] Jung R, Kim HS, Kim Y, et al. Electrically conductive transparent papers using multiwalled carbon nanotubes. Journal of Polymer Science Part B: Polymer Physics. 2008;**46**(12): 1235-1242

[12] Tian H, Yang Y, Xie D, et al. A novel flexible capacitive touch pad based on graphene oxide film. Nanoscale. 2013; **5**(3):890-894

[13] Malara F, Manca M, Marco LD, et al. Flexible carbon nanotube-based composite plates as efficient monolithic counter electrodes for dye solar cells. ACS Applied Materials & Interfaces. 2011;**3**(9):3625

[14] Hecht DS, Hu L, Irvin G. Emerging transparent electrodes based on thin films of carbon nanotubes, graphene, and metallic nanostructures. Advanced Materials. 2011;**23**(13):1482-1513

[15] Brennan LJ, Byrne MT, Bari M, et al. Carbon nanomaterials for dye-sensitized solar cell applications: A bright future. Advanced Energy Materials. 2011;**1**(4):472-485

[16] Hu L, Hecht D, Grüner G. Percolation in transparent and conducting carbon nanotube networks. Nano Letters. 2014;**4**(12):2513-2517

[17] Meng Y, Xu XB, Li H, et al. Optimisation of carbon nanotube ink for large-area transparent conducting films fabricated by controllable rod-coating method. Carbon. 2014;**70**(2):103-110

[18] Tenent RC, Barnes TM, Bergeson JD, et al. Ultrasmooth, large-area,

high-uniformity, conductive transparent single-walled-carbon-nanotube films for photovoltaics produced by ultrasonic spraying. Advanced Materials. 2010; **21**(31):3210-3216

[19] Wang J, Liang M, Fang Y, et al. Rod-coating: Towards large-area fabrication of uniform reduced graphene oxide films for flexible touch screens. Advanced Materials. 2012;**24**(21): 2874-2878

[20] Hellstrom SL, Lee HW, Bao Z. Polymer-assisted direct deposition of uniform carbon nanotube bundle networks for high performance transparent electrodes. ACS Nano. 2009;**3**(6):1423-1430

[21] Parekh BB, Fanchini G, Eda G, et al. Improved conductivity of transparent single-wall carbon nanotube thin films via stable postdeposition functionalization. Applied Physics Letters. 2007;**90**(12):2513

[22] Fukaya N, Dong YK, Kishimoto S, et al. One-step sub-10 μm patterning of carbon-nanotube thin films for transparent conductor applications. ACS Nano. 2014;**8**(4):3285-3293

[23] Trung TQ, Ramasundaram S, Hong SW, et al. Flexible and transparent nanocomposite of reduced graphene oxide and P(VDF-TrFE) copolymer for high thermal responsivity in a field-effect transistor. Advanced Functional Materials. 2014; **24**(22):3438-3445

[24] Kim SH, Song W, Jung MW, et al. Carbon nanotube and graphene hybrid thin film for transparent electrodes and field effect transistors. Advanced Materials. 2014;**26**(25):4247-4252

[25] Wu Z, Chen Z, Du X, et al. Transparent, conductive carbon nanotube films. Science. 2004; **305**(5688):1273-1276

[26] Guo P, Song H, Chen X. Electrochemical performance of graphene nanosheets as anode material for lithium-ion batteries. Electrochemistry Communications. 2009;**8**(1):137-142

[27] Cao X, Chuan X, Li S, et al. Hollow silica spheres embedded in a porous carbon matrix and its superior performance as the anode for lithium-ion batteries. Particle & Particle Systems Characterization. 2016;**33**(2): 110-117

[28] Yang Y, Wang Z, Zhou Y, et al. Synthesis of porous Si/graphite/carbon nanotubes@C composites as a practical high-capacity anode for lithium-ion batteries. Materials Letters. 2017;**199**: 84-87

[29] Ma T, Yu X, Li H, et al. High volumetric capacity of hollow structured SnO_2@Si nanospheres for lithium-ion batteries. Nano Letters. 2017;**17**(6):3959

[30] An W, Fu J, Mei S, et al. Dual carbon layers hybridized mesoporous tin hollow spheres for fast-rechargeable and high-stable lithium-ion battery anode. Journal of Materials Chemistry A. 2017;**5**(27)

[31] Jeong MG, Du HL, Islam M, et al. Self-rearrangement of silicon nanoparticles embedded in micro-carbon sphere framework for high-energy and long-life lithium-ion batteries. Nano Letters. 2017;**17**(9)

[32] Iijima S. Helical microtubules of graphitic carbon. Nature. 1991; **354**(6348):56-58

[33] Yoon S, Lee S, Kim S, et al. Carbon nanotube film anodes for flexible lithium ion batteries. Journal of Power Sources. 2015;**279**:495-501

[34] Chen S, Shen L, Peter A, et al. Dual-functionalized double carbon shells

coated silicon nanoparticles for high performance lithium-ion batteries. Advanced Materials. 2017:1605650

[35] Ye H, Xin S, Yin YX, et al. Advanced porous carbon materials for high-efficient lithium metal anodes. Advanced Energy Materials. 2017: 1700530

[36] Luo F, Chu G, Xia X, et al. Thick solid electrolyte interphases grown on silicon nanocone anodes during slow cycling and their negative effects on the performance of Li-ion batteries. Nanoscale. 2015;**7**(17):7651

[37] Wang H, Li Z, Ghosh K, et al. Synthesis of double-walled carbon nanotube films and their field emission properties. Carbon. 2010;**48**(10): 2882-2889

[38] Shinke K, Ando K, Koyama T, et al. Properties of various carbon nanomaterial surfaces in bilirubin adsorption. Colloids & Surfaces B: Biointerfaces. 2010;**77**(1):18-21

[39] Ghosh K, Kumar M, Maruyama T, et al. Micro-structural, electron-spectroscopic and field-emission studies of carbon nitride nanotubes grown from cage-like and linear carbon sources. Carbon. 2009;**47**(6):1565-1575

[40] Beaulieu LY, Hatchard TD, Bonakdarpour A, et al. Reaction of Li with alloy thin films studied by in situ AFM. Journal of the Electrochemical Society. 2003;**150**(11):A1457-A1464

[41] Wada T, Ichitsubo T, Yubuta K, et al. Bulk-nanoporous-silicon negative electrode with extremely high cyclability for lithium-ion batteries prepared using a top-down process. Nano Letters. 2014;**14**:4505-4510

[42] Lv Q, Liu Y, Ma T, et al. Hollow structured silicon anodes with stabilized solid electrolyte interphase film for lithium-ion batteries. ACS Applied Materials & Interfaces. 2015;**7**: 23501-23506

[43] Sun XG, Qiu ZW, Chen L, et al. Industrial synthesis of Whisker carbon nanotubes. Materials Science Forum. Trans Tech Publications Ltd. 2016; **852**:514

[44] Huang X, Yang J, Mao S, et al. Controllable synthesis of hollow Si anode for long-cycle-life lithium-ion batteries. Advanced Materials. 2014; **26**(25):4326-4332

[45] Ma H, Cheng F, Chen J, et al. Nest-like silicon nanospheres for high-capacity lithium storage. Advanced Materials. 2010;**19**(22):4067-4070

[46] Zhou XY, Tang JJ, Yang J, et al. Silicon@carbon hollow core–shell heterostructures novel anode materials for lithium-ion batteries. Electrochimica Acta. 2013;**87**(1):663-668

[47] Sheng L, Jin A, Yu L, et al. A simple and universal method for fabricating linear carbon chains in multiwalled carbon nanotubes. Materials Letters. 2012;**81**(3):222-224

[48] Ghosh K, Kumar M, Maruyama T, et al. Tailoring the field emission property of nitrogen-doped carbon nanotubes by controlling the graphitic/pyridinic substitution. Carbon. 2010; **48**(1):191-200

[49] Ghosh K, Kumar M, Maruyama T, et al. Microstructural, electron-spectroscopic and field-emission studies of carbon nitride nanotubes grown from cage-like and linear carbon sources. Carbon. 2009;**47**:1565-1575

[50] Andoa K, Shinkea K, Yamadaa S, Koyamab T, et al. Fabrication of carbon nanotube sheets and their bilirubin adsorption capacity. Colloids and Surfaces B: Biointerfaces. 2009;**71**(2): 255-259

[51] Kumar M, Ando Y. Camphor—A botanical precursor producing garden of carbon nanotubes. Diamond & Related Materials. 2003;**12**:998-1002

[52] Shimizu T, Abe H, Ando A, et al. Electric transport measurement of a multi-walled carbon nanotube in scanning transmission electron microscope. Physica E: Low-dimensional Systems and Nanostructures. 2004;**24**:37-41

[53] Taniguchi M, Nagao H, Hiramatsu M, et al. Preparation of dense carbon nanotube film using microwave plasma-enhanced chemical vapor deposition. Diamond & Related Materials. 2005; **14**(1):855-858

[54] Endo M et al. Stacking nature of graphene layers in carbon nanotubes and nanofibres. Journal of Physics & Chemistry of Solids. 1997;**58**(11): 1707-1712